An Analytical Approach of Bubble Departure by Sliding in Vertical Flow Boiling

Luc Favre, Stéphane Pujet, Stéphane Mimouni, Catherine Colin

An Analytical Approach of Bubble Departure by Sliding in Vertical Flow Boiling

Luc FAVRE, Stéphane PUJET, and Stéphane MIMOUNI
Mécanique des Fluides, Énergie et Environement, EDF R&D
6 Quai Watier, 78401 Chatou, FRANCE
luc.favre@edf.fr; stephane.pujet@edf.fr; stephane.mimouni@edf.fr

Catherine COLIN
Institut de Mécanique des Fluides de Toulouse
Université de Toulouse, CNRS INP_UPS
2 Allée du Professeur Camille Soula, 31400 Toulouse, FRANCE
catherine.colin@toulouse-inp.fr
doi.org/10.13182/126-38201

ABSTRACT

Bubble departure by sliding is a quasi-systematically observed phenomenon in vertical flow boiling. The prediction of the diameter at which bubble sliding begins is required if one wishes to properly model the wall boiling phenomenon, which is a primal goal in the nuclear industry. An approach based on recent expressions for the force balance such as drag and added mass is proposed. The dimensionless analysis provides a way to determine dominant forces triggering departure in experimental measurements at low and high pressures. While added mass seems to be the stronger detaching force at atmospheric pressure, drag appears to be the dominant one when pressure increases. Predictions of departure diameter through a critical radius in the dimensionless force balance shows a reasonable trend with experimental data while having a reduced number of arbitrary choices in the modeling compared to other existing approaches. The proposed work will be applied to the lift-off phenomenon and could be enriched with more experimental measurements as well as finer modeling of the bubble growth by accounting for liquid subcooling and liquid temperature field.

KEYWORDS
nucleate boiling, force balance, sliding, departure diameter, dimensionless analysis

1 INTRODUCTION

Studying the physics of boiling is a major topic related to many industrial fields, notably in the nuclear industry where boiling can both improve the heat transfer or become a safety issue when the **Critical Heat Flux** (CHF) is reached. The CHF is the heat flux at which a transition occurs between nucleate boiling and film boiling over the heater's surface, a phenomenon called the **boiling crisis** or the **Departure from Nucleate Boiling** (DNB). This transition is nearly instantaneous and can severely damage the heater since film boiling drastically reduces the global heat transfer coefficient and leads to a rapid rise of the wall temperature.

Aware of such a phenomenon, it is then of primal importance for nuclear reactor operators to be able to predict the CHF in any conditions to prevent the occurence of the boiling crisis.

To do so, recent numerical methods using **Computational Multi Fluids Dynamics** (CMFD) are becoming increasingly considered to estimate the local thermal-hydraulics conditions in order to propose dedicated

modelings of the boiling phenomenon at small scales to predict the evolution of the wall temperature depending on the applied heat flux.

Historically, first approaches consisted of experimental correlations established in various flow conditions to directly relate the wall temperature to the wall heat flux [1]. Nowadays, more advanced models consider a **Heat Flux Partitioning** (HFP) which consists of splitting the total wall heat flux into different contributions related to specific physical heat transfer phenomena. The pioneering work of Kurul & Podowski [2] considered three mechanisms : liquid forced convection (convective heat transfer), phase change (boiling heat transfer) and rewetting of the surface, leading to transient heat transfer after bubble lift-off (quenching).

However, HFP models show several drawbacks which can be tackled in different ways. First, the estimation of each flux requires closure relationships for numerous parameters (nucleation site density, bubble lift-off diameter, bubble departure frequency, etc.) which make them very sensitive to the chosen laws. Moreover, recent works on the HFP models proposed to extend the considered mechanisms in order to account for additional phenomena such as bubble sliding on the wall [3], bubble microlayer evaporation [4] or condensation at bubble top [5].

A previous work conducted using NEPTUNE_CFD [6], the CMFD code developed by EDF R&D to simulate multiphase flows, showed that simply changing the nucleation site density correlation in the implemented HFP model reduced by 30% the error on the wall temperature prediction [7] for vertical flows of R12 [8]. This result motivated the development of a new HFP model aimed to be implemented in the code.

In this framework, the present study aims to contribute to the description of the bubble departure by sliding mechanism through an analysis of the force balance on a single bubble nucleating on a vertical wall. Section 2 will recall the main features of bubble dynamics on a wall along with the chosen expression of each forces. Section 3 presents a dimensionless approach to evaluate dominant forces responsible for sliding. Then, Section 4 compares predictions of bubble departure diameter using the dimensionless force balance against exprimental measurements. Section 5 finally draws conclusions and perspectives regarding the presented approach and wall boiling modeling.

2 NUCLEATING BUBBLE DYNAMICS IN VERTICAL UPWARD FLOWS

2.1. Recent Experimental and Numerical Insights / Previous Approaches

Dynamics of bubbles in vertical flows is an active field of research since decades. Many experimental visualizations of single bubbles in different flow conditions have been conducted by various authors both for air-injected growth in a shear flow [9] and saturated or subcooled flow boiling [10–12]. Those investigation works are insightful to determine the dynamic mechanisms that trigger the sliding or the lift-off of the bubble.

For instance, many authors have noticed that in vertical boiling, bubbles rapidly detach from their nucleation site and spend most of their lifetime sliding on the wall before lifting-off. This results in a significant impact on the local heat transfer due to the thermal footprint in the bubble's wake [13]. Moreover, measurements of quantities such as bubble diameters associated to departure by sliding and lift-off are of great interest to validate models based on force balance equations [14, 15].

One can also refer to experimental studies of flat plate subcooled flow boiling, in which hundreds of nucleating bubbles are observed simultaneously to determine, for instance, time and statistical averaged bubble diameter and velocity over very large range of flow conditions representative of industrial configurations [16, 17]. In particular, recent high-pressure observations confirmed that bubbles size dramatically decreases from roughly 1mm at 1 Bar to 0.01mm at 40 Bar and that their lifetime increases with longer sliding distances.

Strong advances in numerical methods and simulations are also of great interest to study bubble dynamics. For instance, **Direct Numerical Simulations** (DNS) of growing spherical bubbles in uniform flow [18], hemispherical bubble sliding on a wall [19] or even of a spherical bubble in a shear flow at various distance of a wall [20] allow to numerically study the hydrodynamic efforts experienced by the bubble in various conditions. Such works often result in correlated expressions of forces such as drag, lift or added mass effects with the advantage of accounting for different flow conditions and features being either inertial effects, shear effects or wall vicinity.

Thanks to those insights offered by both experimental an numerical works since the end of the 1980's, researchers started to propose mechanistic approaches to try to predict bubble departure and lift-off diameters using a force balance [14, 15]. The main idea behind those models is to compute the whole force balance on a bubble during its growth and to define criteria for detachment and / or lift-off and numerically deduce the associated diameters.

Such approaches use point-force equations for spherical bubbles and already showed reasonable agreement with experimental measurements and trends depending on the flow conditions (wall heat flux / superheat, liquid mass flux, etc.). However, the associated forces' expressions are often validated for simple conditions such as unbounded liquid medium in a limited range of bubble Reynolds number.

The precise derivation of the whole force balance for an arbitrary bubble on a wall in any flow conditions remains a very difficult task, if not impossible. Our goal here is to follow a similar approach and to propose enhanced descriptions of the forces using recent expressions to tentatively make a step towards the real physical situation experienced by the bubble.

2.2. Force Balance Representation in Vertical Flow Boiling

We consider a bubble nucleating on a vertical wall with a inclination $\mathrm{d}\theta$ compared to its static contact angle θ and facing an upward flow (Figure 1). The shape is supposed to be quasi-spherical, based on the fact that most forces would not have a known expression if we considered an arbitrary bubble shape.

The force balance on the bubble includes :

- The surface tension or capillary force $\overline{F_C}$, occurring at the triple contact line ;
- The contact pressure force $\overline{F_{CP}}$, arising from the pressure difference at the interface ;
- The buoyancy $\overline{F_B}$, due to the gravity $\overline{g} = -g\,\overline{e_x}$;
- The drag $\overline{F_D}$ and lift $\overline{F_L}$ forces, induced by the liquid stress at the liquid-vapor interface ;
- The added mass force $\overline{F_{AM}}$, related to the displaced masses of fluid when the bubble grows or slides.

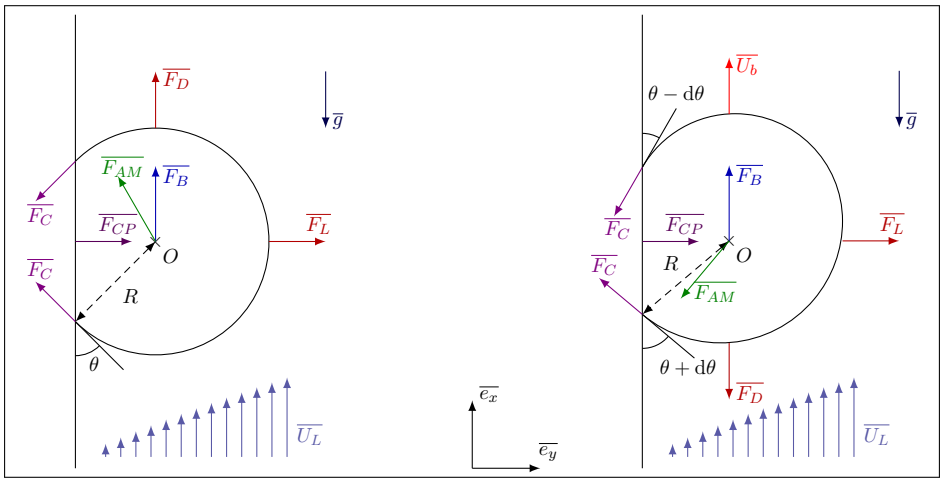

Figure 1. Sketch of a bubble on a vertical wall. Left pictures a static, non-inclined spherical cap bubble. Right pictures a sliding (faster than the liquid, occurring sometimes under buoyancy and drag effects) and inclined bubble with a shape close to a truncated sphere.

Respecting Newton's second law, if the bubble is static or slides at a constant velocity, we have :

$$\overline{F_C} + \overline{F_{CP}} + \overline{F_B} + \overline{F_D} + \overline{F_L} + \overline{F_{AM}} = \overline{0} \tag{1}$$

2.2.1. Buoyancy force

The buoyancy force is equal to :

$$\overline{F_B} = V_b \left(\rho_V - \rho_L\right) \overline{g} = V_b \left(\rho_L - \rho_V\right) g \, \overline{e_x} \tag{2}$$

2.2.2. Capillary force

The capillary force results of the integration of the effort $\sigma\overline{\tau}$ exerted at the triple contact line over the foot radius r_w. Following the approach of Klausner [10] and defining $\theta_u = \theta + \mathrm{d}\theta$ and $\theta_d = \theta - \mathrm{d}\theta$, we obtain :

$$\overline{F_C} = -\pi R\sigma \left[1.25 \, \frac{2\mathrm{d}\theta}{\left(\frac{\pi}{2}\right)^2 - \mathrm{d}\theta^2} \sin\left(\theta\right)^2 \cos\left(\mathrm{d}\theta\right)^2\right] \overline{e_x} - \pi R\sigma \left[2 \sin\left(\theta\right)^2 \frac{\sin\left(2\mathrm{d}\theta\right)}{2\mathrm{d}\theta}\right] \overline{e_y} \tag{3}$$

where σ is the surface tension and $r_w \approx R \, \dfrac{\sin\left(\theta_u\right) + \sin\left(\theta_d\right)}{2} = R \sin\left(\theta\right) \cos\left(\mathrm{d}\theta\right)$.

2.2.3. Contact pressure force

The contact pressure force, arising from the pressure jump at the liquid-vapor interface is expressed by integrating the associated effort over the bubble's foot surface πr_w^2. Using Laplace equation for the

pressure difference and noting R_c the bubble's curvature radius :

$$\overline{F_{CP}} \approx \frac{2\sigma}{R_c}\pi r_w^2\,\overline{e_y} \approx \pi R\sigma\; 2\sin(\theta)^2\cos(\mathrm{d}\theta)^2\;\overline{e_y} \tag{4}$$

where $R_c = R$ in the case of a truncated sphere.

It is important to note that in many force balance modeling, some authors write $R_c = C \times R$ with $C > 1$ [15] to adjust the contact pressure magnitude, without any further justification.

2.2.4. Drag and lift Forces

The drag and lift forces are defined as the tangential and normal components of the total hydrodynamic effort computed by integrating the liquid stress tensor over the bubble's surface. Associated drag and lift coefficients C_D and C_L are then defined by :

$$\overline{F_D} = \frac{1}{2}C_D\rho_L S_p\left(\overline{U_L} - \overline{U_b}\right)\left|\left|\overline{U_L} - \overline{U_b}\right|\right| \quad ; \quad \overline{F_L} = \frac{1}{2}C_L\rho_L S_p\left(\overline{U_L} - \overline{U_b}\right)^2\;\overline{e_y} \tag{5}$$

where ρ_L is the liquid density and S_p the projected area of the bubble in the direction of the flow.

Shi *et al.* proposed novel expressions for C_D and C_L correlated using results from DNS of a shear flow over a spherical bubble near a wall for bubble Reynolds number varying from 10^{-1} to 10^3. Those coefficients depend mostly on the bubble Reynolds number $\mathrm{Re}_b = 2R\left|U_{rel}\right|/\nu_L$, the shear rate $\mathrm{Sr} = \gamma\, 2R/\left|U_{rel}\right|$ and the non-dimensional distance to the wall $L_R = y/R$ with $U_{rel} = \left(\overline{U_L} - \overline{U_b}\right)\cdot\overline{e_x}$; $\gamma = \dfrac{\partial U_{rel}}{\partial y}\,(y = R)$ and y the distance between the wall and the bubble's center.

They propose a correction of the drag coefficient ΔC_D to account for wall and shear effect, defined as :

$$C_D = C_{D,U0}\left(1 + \Delta C_D\right) \tag{6}$$

where $C_{D,U0}$ is the drag coefficient in an unbounded liquid, computed following Mei *et al.* [21] :

$$C_{D,U0} = \frac{16}{\mathrm{Re}_b}\left[1 + \frac{3}{2}\left(\left(\frac{12}{\mathrm{Re}_b}\right)^n + 0.796^n\right)^{-1/n}\right] \quad ; \quad n = 0.65 \tag{7}$$

Shi *et al.* derived the following correlation for the drag correction :

$$\Delta C_D = \Delta C_D\left[\mathrm{Re}_b = O(1)\right] + \left(1 - e^{-0.07\mathrm{Re}_b}\right)\Delta C_D\left[\mathrm{Re}_b \gg 1\right] \tag{8}$$

$$\Delta C_D\left[\mathrm{Re}_b = O(1)\right] = \frac{\left[1 + \tanh\left(0.012\mathrm{Re}_b^{0.8}\right) + \tanh\left(0.07\mathrm{Re}_b^{0.8}\right)\right]^2}{1 + 0.16L_u\left(L_u + 4\right)} \times \left[\left(\frac{3}{8}L_R^{-1} + \frac{3}{64}L_R^{-4}\right)\left(1 - \frac{3}{8}L_R^{-1} - \frac{3}{64}L_R^{-4}\right)^{-1} - \frac{1}{16}\left(L_R^{-2} + \frac{3}{8}L_R^{-3}\right)\mathrm{Sr}\right] \tag{9}$$

$$\text{where } L_u = y\frac{\left|U_{rel}\right|}{\nu_L} \tag{10}$$

$$\Delta C_D\left[\mathrm{Re}_b \gg 1\right] = 0.47L_R^{-4} + 0.0055L_R^{-6}\mathrm{Re}_b^{3/4} + 0.002\left|\mathrm{Sr}\right|^{1.9}\mathrm{Re}_b + 0.05L_R^{-7/2}\mathrm{Sr}\mathrm{Re}_b^{1/3} \tag{11}$$

For the sake of concision, we do not detail the full computation of the lift coefficient C_L and refer the reader to Shi *et al.* original paper [20]. We just mention that their approach consists of summing three lift contributions respectively linked to the wall presence, the shear and their coupling. Both contributions are expressed using correlations with the previously detailed quantities. In particular, their expression of C_L detects a change in the lift direction when reaching negative values of Sr or high Re_b values when Sr is small.

It is important to note that their correlation are based on numerical simulations down to $L_R = 1.5$, which is the smallest value of the wall distance for which they conducted DNS. However, Scheiff *et al.* [22] measured experimental drag coefficient of bubbles sliding on a wall and compared it with Shi *et al.* expression extended to $L_R = 1$ (spherical bubble laying on a wall) which resulted in a good agreement between predicted and measured values.

2.2.5. Added mass force

To compute the added mass force experienced by the bubble while growing and sliding on the wall, we use the expression of the total liquid kinetic energy derived by Van Der Geld [23] in the case of a potential flow around a growing sphere laying on a wall with a uniform incoming liquid velocity. This expression of the liquid kinetic energy is then injected in Lagrange's equations to derive the total added mass force exerted on the bubble in both directions [24] :

$$\frac{\overline{F_{AM}}}{\rho_L V_0} = \left(C_{AM,x1} \frac{\dot{R}}{R} U_{rel} + C_{AM,x2} \frac{\partial U_b}{\partial t} \right) \overline{e_x} + \left(C_{AM,y1} \frac{\dot{R}^2}{R} + C_{AM,y2} \ddot{R} + C_{AM,y3} \frac{U_{rel}^2}{R} \right) \overline{e_y} \quad (12)$$

with $V_0 = 4\pi R^3/3$ and the estimated added mass coefficients $C_{AM,x1} \approx 1.9089$, $C_{AM,x2} \approx -0.63629$, $C_{AM,y1} \approx -1.1356$, $C_{AM,y2} \approx -0.2699$ and $C_{AM,y3} \approx 0.00877$.

We can note that parallel to the wall, the coupled term $\dot{R}U_{rel}$ will tend to *promote detachment and sliding* of the bubble if $U_{rel} > 0$ (which is the case if the bubble is still attached to its nucleation site). This strongly *contrasts with former approaches* where authors chose to rely on Rayleigh-Plesset equation of bubble growth in a quiescent unbounded liquid by projecting the total force along both axes using the inclination angle of the bubble. Such assumptions lead to an added mass parallel to the wall hindering detachment at early stage of bubble growth, which appears to be unphysical compared to the results using potential flow theory including the liquid velocity and the wall.

3 BUBBLE DEPARTURE BY SLIDING

3.1. Dominant Forces at Departure by Sliding

Once each forces has been described, we can write the whole force balance parallel to the wall for a bubble prior to the departure by sliding. Since we further need expressions for R and $\dot{R}$, we suppose $R(t) = K\mathrm{Ja}_w\sqrt{\eta_l t}$ with $K \approx 2$ for the early stage of bubble growth as proposed and validated in different research works [10, 25]. Before departure, we have $\overline{U_b} = \overline{0}$. The total force balance parallel to the wall then yields :

$$-\pi R\sigma f_{C,x}(\theta, \mathrm{d}\theta) + V_b(\rho_L - \rho_V) g + \frac{1}{2} C_D \rho_L S_p U_L^2 + \rho_L V_0 C_{AM,x1} \frac{\dot{R}}{R} U_L = 0 \quad (13)$$

with $f_{C,x} = 2.5\,\dfrac{\mathrm{d}\theta}{(\pi/2)^2 - \mathrm{d}\theta^2}\sin(\theta)^2\cos(\mathrm{d}\theta)^2 \to 0$ if $\mathrm{d}\theta \to 0$; $V_b = V_0 = \frac{4}{3}\pi R^3$ and $S_p = \pi R^2$.

We re-write this equation in a dimensionless form, dividing the LHS by the added-mass term :

$$-\frac{3}{2}\frac{f_{C,x}}{K^2 C_{AM,x1}}\frac{1}{\mathrm{Ca}}\frac{\mathrm{Pr}}{\mathrm{Ja}_w^2} + \frac{1}{K^2 C_{AM,x1}}\frac{\mathrm{Re}_b}{\mathrm{Fr}}\frac{\mathrm{Pr}}{\mathrm{Ja}_w^2} + \frac{3}{8}\frac{C_D}{K^2 C_{AM,x1}}\mathrm{Re}_b\frac{\mathrm{Pr}}{\mathrm{Ja}_w^2} + 1 = 0 \tag{14}$$

where we have the following non-dimensional numbers :

$$\mathrm{Re}_b = \frac{2RU_L}{\nu_L} \;;\; \mathrm{Fr} = \frac{\rho_L U_L^2}{(\rho_L - \rho_V)\,gR} = \mathrm{Re}_b^2\frac{\rho_L \nu_L^2}{g\,(\rho_L - \rho_V)\,4R^3} \;;\; \mathrm{We} = \frac{\rho_L U_L^2 R}{\sigma} \;;\; \mathrm{Eo} = \frac{(\rho_L - \rho_V)\,gR^2}{\sigma}$$
$$\mathrm{Ja}_w = \frac{(T_w - T_{sat})\,\rho_L c_{P,L}}{\rho_V h_{LV}} \;;\; \mathrm{Pr} = \frac{\nu_L}{\eta_L} \;;\; \frac{\dot{R}}{U_L} = \frac{K^2\mathrm{Ja}_w^2}{\mathrm{PrRe}_b} \;;\; \mathrm{Ca} = \frac{\mu_L U_L}{\sigma} = \mathrm{Re}_b\frac{\nu_L \mu_L}{2R\sigma} \tag{15}$$

Since drag, added mass and buoyancy will promote detachment, we can derive criteria to compare each force's influence in the departure process :

$$\text{Added Mass greater than Drag if :}\;\; \frac{\mathrm{Ja}_w^2}{\mathrm{Pr}} > \frac{3}{8}\frac{C_D}{C_{AM,x1}}\frac{1}{K^2}\mathrm{Re}_b \tag{16}$$

$$\text{Added Mass greater than Buoyancy if :}\;\; \frac{\mathrm{Ja}_w^2}{\mathrm{Pr}} > \frac{1}{C_{AM,x1}K^2}\frac{\mathrm{Re}_b}{\mathrm{Fr}} \tag{17}$$

$$\text{Drag greater than Buoyancy if :}\;\; \mathrm{Re}_b > \frac{16}{3}C_D\frac{\mathrm{Eo}}{\mathrm{Ca}} = \mathrm{Re}_c \tag{18}$$

We can then choose a diameter R and fluid properties to simultaneously plots those criteria on a $\left(\mathrm{Ja}_w^2/\mathrm{Pr}\;;\;\mathrm{Re}_b\right)$ map to visualize predominance ranges as shown on Figure 2.

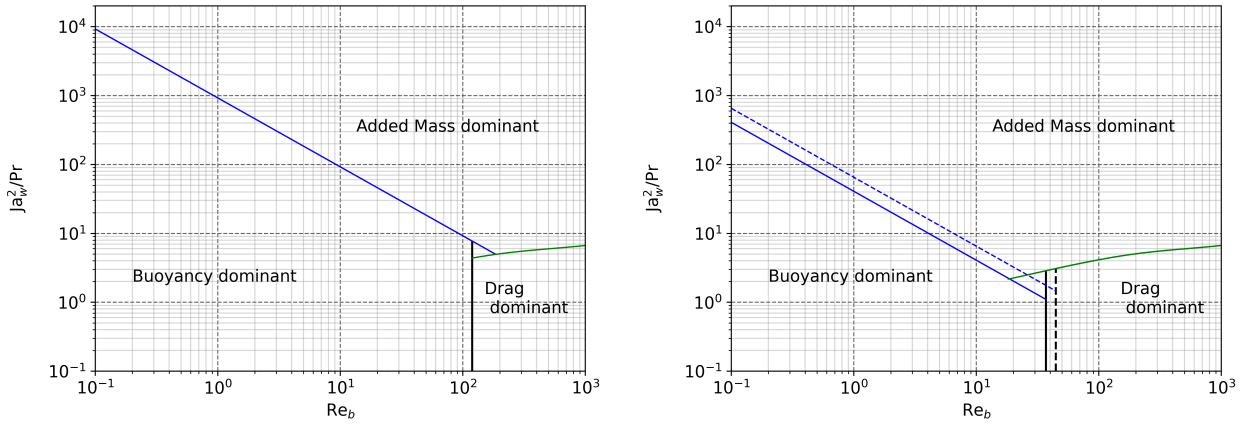

Figure 2. Force predominance map. Green, blue and black lines are respectively conditions (16), (17) and (18). Left represents R =0.25 mm for water at 1 Bar. Right represents R =0.05 mm, water at 150 Bar (plain lines) and R12 at 25 Bar (dashed lines).

It appears that the increase in pressure along with the bubble diameter decrease leads to a larger range of flow parameters for which added mass effects and drag will be dominant. In addition, we also plotted the

conditions for R12 at the similarity pressure of 26 Bar where its properties such as We and ρ_L/ρ_V are close to water in PWR conditions [8]. The proximity between the boundaries on Figure 2 interestingly indicates that *bubbles in pressurized R12 tests are likely to behave very similarly to bubbles in PWR regarding their departure by sliding.*

It is also interesting to note that the frontier between added mass and drag defined by condition (16) remains unchanged for the different pressures, fluids and bubble radii.

3.2. Application to Low Pressure Data

In order to apply the predominance criteria, we gathered three data sets of experimental bubble departure diameter measurements in vertical flow boiling of water at atmospheric pressure. The associated experimental conditions are gathered on Table I.

Table I. Thermal-hydraulics parameters range for the low pressure data.

Author	D_h (mm)	G (kg/m^2/s)	ΔT_w (K)	D_d (mm)	Re_b (-)	$\mathrm{Ja}_w^2/\mathrm{Pr}$ (-)
Sugrue *et al.* [12]	16.642	250 - 400	2 - 6	0.229 - 0.391	53.8 - 70.8	20.57 - 185.2
Guan *et al.* [26]	9	87.3 - 319.2	4.5 - 8.5	0.62 - 1.85	75.9 - 406.02	104.2 - 371.6
Maity [11]	20	0 - 239.6	5 - 5.9	0.788 - 1.713	0 - 241.04	128.6 - 179.06

To further justify the nearly-spherical shape hypothesis, we compute the range of Weber, Capillary and Eotvos numbers since they are representative of the deformability of the bubble under inertial, viscous and gravity effects (Table II).

Table II. Weber, Capillary and Eotvos numbers range for the low pressure data.

Author	We (-)	Ca (-)	Eo (-)
Sugrue *et al.* [12]	6.36×10^{-3} - 12.6×10^{-3}	2.22×10^{-4} - 3.64×10^{-4}	2.09×10^{-3} - 6.09×10^{-3}
Guan *et al.* [26]	3.79×10^{-3} - 82.8×10^{-3}	0.998×10^{-4} - 4.93×10^{-4}	1.53×10^{-2} - 13.6×10^{-2}
Maity [11]	0 - 3.5×10^{-2}	0 - 3.27×10^{-4}	2.48×10^{-2} - 11.7×10^{-2}

To compute the predominance boundaries as done in Figure 2, we need to choose a bubble radius. Here we take the average departure radius of each data set to plot the associated boundaries. It appears that Guan and Maity data sets have very close average departure radius (approx. 0.6 mm) and thus have the same predominance zones. The results are displayed on Figure 3.

It immediately appears that when departure by sliding occurs, 32 measurements out of 37 seem to be dominated by added mass effects. The remaining 5 are buoyancy-dominant (Guan and Maity data) but placed really close to the added mass / buoyancy boundary on the map. This observation tends to indicates

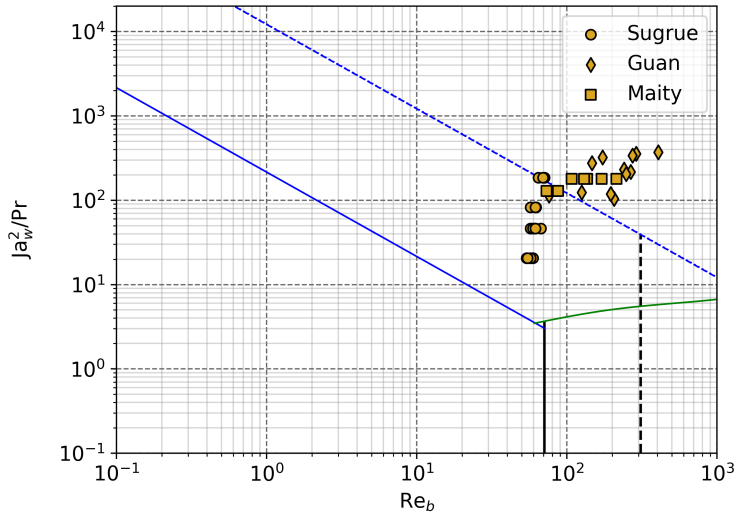

Figure 3. Experimental measurements in the dominance map. Plain lines correspond to Sugrue average departure radius (0.15 mm), dashed lines to Guan and Maity (0.59 mm).

that at low pressure and mass fluxes, the departure by sliding could be triggered mostly by the added mass effects resulting of the coupling between the rapid initial bubble growth and the surrounding liquid velocity (Subsection 2.2.5).

This is mainly a consequence of the significant wall superheat reached in such boiling conditions along with high values of ρ_L/ρ_V, leading to high values of $\mathrm{Ja}_w^2/\mathrm{Pr}$.

3.3. Application to High Pressure Data

Measurements of high-pressure bubble departure diameter are more difficult to find in the literature especially because of the great difficulty to provide clear visualization of individual bubbles when pressure increases, since bubbles are greatly reducing in size down to a few μm.

Nevertheless, recent works such as those conducted by Kossolapov [17] have managed to conduct such measurements at pressures up to 39.8 Bar. To evaluate the forces responsible for sliding at higher pressures, closer to PWR operating conditions, we conduct the same analysis as we did with the low-pressure data. Experimental operations and non-dimensional numbers are summed up in Table III.

Wall superheat or heat flux values are not specified in Kossolapov data because the given diameters were used to depict a global trend with pressure and mass flux. However, wall superheat at **Onset of Nucleate Boiling** can be roughly estimated using Frost & Dzakowic correlation [27] which yields approximately $\Delta T_w \approx 4$ K for water at 40 Bar under a 1 MW/m^2 heat flux. To cover a tentatively large enough range of $\mathrm{Ja}_w^2/\mathrm{Pr}$ values, we will place the measurements from Kossolapov on the predominance map assuming three possible wall superheats : 1 K, 5 K and 10 K.

Table III. Thermal-hydraulics parameters and dimensionless numbers range for Kossolapov data.

Author	D_h (mm)	G (kg/m^2/s)	P (Bar)	D_d (mm)	Re_b (-)
Kossolapov [17]	11.78	500 - 2000	10.5 ; 19.9 ; 39.8	0.01 - 0.13	5.95 - 131.77

We (-)	Ca (-)	Eo (-)
0.5×10^{-3} - 84.8×10^{-3}	1.47×10^{-4} - 14.8×10^{-4}	0.82×10^{-5} - 85×10^{-5}

The resulting map is displayed on Figure 4. In order to make it easier to interpret, we colored the stable added mass / drag boundary (16) in black and used 3 colors to distinguish between the three operating pressures. The arbitrary superheat are made distinct with the markers shapes.

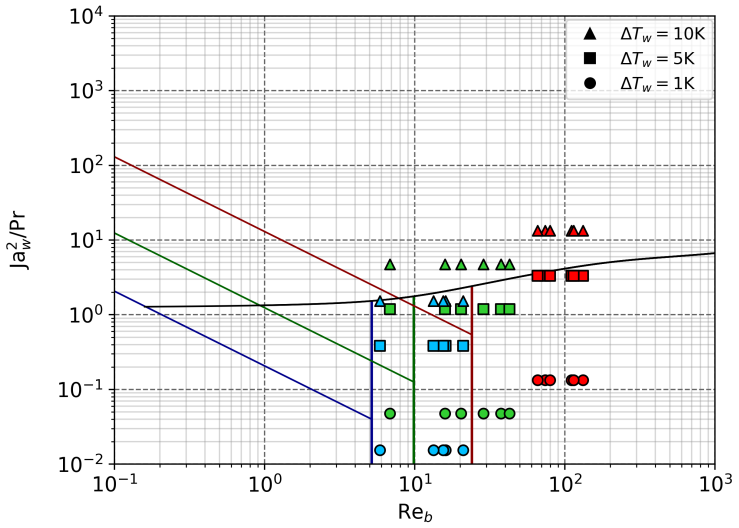

Figure 4. Experimental measurements from Kossolapov in the dominance map. Frontiers are plotted for the average departure radius at the given pressure. Blue : 39.8 Bar - Green : 19.9 Bar - Red : 10.5 Bar.

The main observation here relates to the values of $\mathrm{Ja}_w^2/\mathrm{Pr}$ which appear to be way smaller compared to the low pressure data, even for superheats as high as 10K. This is mainly resulting from the strong decrease in the ρ_L/ρ_V ratio with pressure, thus leading to predominance ranges where the force mostly responsible for departure by sliding is the drag. The higher mass fluxes also tend to increase this effect. Added mass only start to be significant under the 10 K superheat assumption.

Finally, this analysis of high pressure data tends to indicate that *departure by sliding at high pressure is triggered in significantly different dynamic conditions in term of forces ratio (drag dominant) compared to low pressure (added mass dominant).*

4 PREDICTION OF BUBBLE DEPARTURE DIAMETER

The main goal of such a study would still remain to find a way to predict the departure diameter of bubbles in vertical flow boiling. Since only the capillary force is opposed to bubble departure, we can use non-dimensional force balance (14) to search the maximum diameter above which :

$$C_{AM,x}K^2\frac{\mathrm{Ja}_w^2}{\mathrm{Pr}}+\frac{\mathrm{Re}_b}{\mathrm{Fr}}+\frac{3}{8}C_D\mathrm{Re}_b>\frac{3}{2}\frac{f_{C,x}}{\mathrm{Ca}} \tag{19}$$

To compute Re_b and C_D, we use Reichardt's law [28] for the wall liquid velocity and shear at a distance $y = R$. Diameters predictions results are displayed on Figure 5. The supposed wall superheat for Kossolapov data is 1 K.

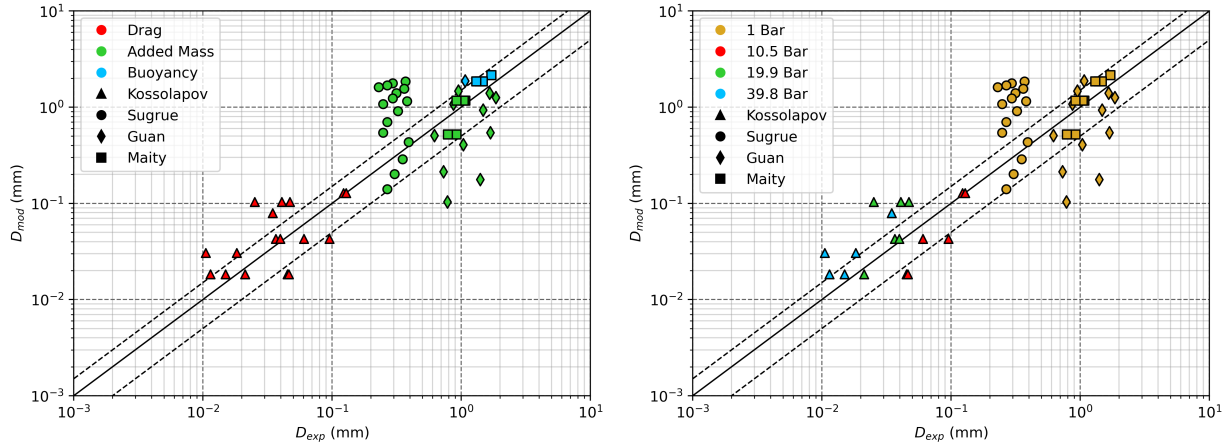

Figure 5. Predicted diameter by Eq. 19 vs. experimental measurements. Colors refer to the dominant force at the departure by sliding (left) or to the operating pressure (right). $\pm 50\%$ error lines in dashed black.

We can see that the predicted diameters seem to reasonably follow the global trend with pressure, which is an important feature in order to distinguish the different dynamic regimes depending on the flow conditions.

The average contact and hysteresis angle used in the computations are $\theta = 45°$, $\mathrm{d}\theta = 36°$ for Sugrue's data (maximum hysteresis observed in her experiments) yielding an average error of 230.4% ; $\theta = 53°$, $\mathrm{d}\theta = 27°$ for Guan's data (maximum hysteresis measured, accounting for uncertainties) yielding an average error of 182% ; $\theta = 60°$, $\mathrm{d}\theta = 20°$ for Maity's data (average static angle, but increased hysteresis compared to the measurements) for an average error of 29.2% ; $\theta = 45°$, $\mathrm{d}\theta = 1°$ for Kossolapov's data for an average error of 53.8% (no measurements available).

Although the results seem to follow a correct trend with pressure, the average error can still be considered high on some data compared to other models [10]. However, such models often chose arbitrary values for parameters like the bubble foot diameter ($d_w = D/15$) [15] or the contact, hysteresis and inclination angles. Recent studies emphasized that such assumptions were substiantially wrong [29]. Moreover, those models consider an opposite contribution of the added mass regarding departure which seems to be incorrect as discussed earlier (Subsection 2.2.5).

In this work, we insisted on keeping straight assumptions of a quasi-spherical bubble and to tried to apply the resulting laws for departure diameter prediction. **The only hypothetically free parameters were the average contact angle and hysteresis.** We tried to use author's data when available as inputs in our model. However, we did not have such measurements for Kossolapov's data and thus chose an average contact angle close to water FTO static contact angle (heater material used in his experiments) along with a very small hystersis, since very small bubbles in highly pressurized flow will be likely to keep non-deformed shapes because of surface tension effects getting stronger as the bubble diminishes in size. Moreover, we had to set a wall superheat which we chose to be $1\mathrm{K}$ (strongly drag-dominant regime).

Concerning the low pressure data, we observed that better results were obtained on Maity's measurements when using a bigger hysteresis angle. This may originate from the bubble foot diameter modeling, which was observed to be lower than the associated truncated sphere foot diameter in his experiments. In addition, the three low pressure data sets (Table I) have very close flow conditions, but significantly different measured departure diameter, especially when comparing Sugrue to Guan and Maity. The observed differences in experimental measurements can thus originate from the heater material, which impact is only indirectly included through the contact angle and hysteresis. This can explain the over-estimation of departure diameter on Sugrue's data when good agreement is observed with Guan and Maity. The same goes for the under-estimated diameters on Guan's data when we have a good agreement with Sugrue's measurements, explaining the high average relative deviation on those data sets.

5 CONCLUSIONS & PERSPECTIVES

In this work, we tried to propose an analytical approach to further understand the quasi-systematically observed departure by sliding phenomenon in vertical flow boiling.

We proposed a reassessed force balance using recent DNS results to better estimate the drag for a bubble laying close to a wall along with a proper derivation of the added-mass force parallel to the wall using potential flow theory.

The analysis of the global force balance in a non-dimensional form showed that number such as $\mathrm{Ja}_w^2/\mathrm{Pr}$ and Re_b are critical to determine the dynamic regime under which bubbles start to slide. We exhibited a predominance map which appeared to be a useful tool to qualitatively study the departure by sliding process under various thermal-hydraulics conditions.

Applying this approach to experimental measurements interestingly indicated that bubble sliding seem to mostly originate from added-mass effects at low pressure and from viscous drag at high pressure. This difference can be explained by the decrease in bubble size and phase density ratio with increasing pressure. The fact that drag may be the truly domining force at high pressure could be of interest to simplify bubble departure modeling for PWR flows. To further investigate this effect, more experimental measurements in representative conditions would be needed.

The non-dimensional force balance was used to compute a critical bubble radius above which the contributing forces systematically overcome the capillary force. This led to bubble departure diameter predictions which appeared to follow a reasonable trend with pressure, with an average error around 50% for high-pressure data.

Still, this approach could be improved in many different ways. First, the chosen growth law is purely based

on diffusive heat transfer and is assumed to be at constant liquid temperature in the early stage of bubble lifetime. This could be enhanced by accounting for bulk liquid subcooling, which has currently no influence in this approach. Moreover, no microlayer evaporation was considered since the occurrence of microlayer regime depends on the flow conditions and seem to disappear when reaching moderate pressures [17]. Taking this microlayer into account for low pressure data may be a way of better predict the added-mass effect induced in departure.

Another way of improvement lies in the prediction of the bubble foot radius, contact angles and curvature radius. The knowledge of an apppropriate hysteresis depending on bubble size and flow conditions could be of great interest in that matter. *The observation that using a very small hysteresis better fits the high-pressure data seem to indicate that the anticipated behavior of low-deforming bubbles at high pressure is reasonable.* Moreover, using an average contact angle and hysteresis for a whole set of measurements could be inappropriate and distinct measurements conducted for each test would help to leverage this uncertainty.

Finally, the approach developed in this paper will be further conducted to analyze the bubble lift-off after sliding. Since less forces are at stake normal to the wall, the resulting analysis would only compare lift, capillary and added-mass forces. This is a currently undergoing work as a continuation of the presented results.

REFERENCES

1. Z. Liu and R. H. Winterton, "A general correlation for saturated and subcooled flow boiling in tubes and annuli, based on a nucleate pool boiling equation," *International Journal of Heat and Mass Transfer*, **34** (11), pp. 2759–2766 (1991).

2. N. Kurul and M. Z. Podowski, "Multidimensional Effects in Forced Convection Subcooled Boiling," *Proc. Proceedings of the 9th Heat Transfer Conference*, pp. 21–26, (1990).

3. N. Basu, G. R. Warrier, and V. K. Dhir, "Wall heat flux partitioning during subcooled flow boiling: Part 1 - Model development," *Journal of Heat Transfer*, **127** (2), pp. 131–140 (2005).

4. L. Gilman and E. Baglietto, "A self-consistent, physics-based boiling heat transfer modeling framework for use in computational fluid dynamics," *International Journal of Multiphase Flow*, **95**, pp. 35–53 (2017).

5. P. Zhou, S. Hua, C. Gao, D. Sun, and R. Huang, "A mechanistic model for wall heat flux partitioning based on bubble dynamics during subcooled flow boiling," *International Journal of Heat and Mass Transfer*, **174** (2021).

6. A. Guelfi et al., "NEPTUNE: A new software platform for advanced nuclear thermal hydraulics," *Nuclear Science and Engineering*, **156** (3), pp. 281–324 (2007).

7. L. Favre, S. Pujet, S. Mimouni, and C. Colin, "NEPTUNE_CFD Simulations of DEBORA-Promoteur Experiments : Boiling Freon in a Vertical Pipe with Mixing Vanes," *Proc. 19th International Topical Meeting on Nuclear Reactor Thermal Hydraulics (NURETH-19)*, pp. 1–17, (2022).

8. J. Garnier, É. Manon, and G. Cubizolles, "Local measurements on flow boiling of refrigerant R12 in a vertical tube," in *Multiphase Science and Technology, Vol. 13*, pp. 1–111, (2001).

9. G. Duhar and C. Colin, "Dynamics of bubble growth and detachment in a viscous shear flow," *Physics of Fluids*, **18** (077101) (2006).

10. J. F. Klausner, R. Mei, D. M. Bernhard, and L. Z. Zeng, "Vapor bubble departure in forced convection boiling," *International Journal of Heat and Mass Transfer*, **36** (3), pp. 651–662 (1993).

11. S. Maity, *Effect of velocity and gravity on bubble dynamics*, PhD thesis, 2000.

12. R. Sugrue, J. Buongiorno, and T. McKrell, "An experimental study of bubble departure diameter in subcooled flow boiling including the effects of orientation angle, subcooling, mass flux, heat flux, and pressure," *Nuclear Engineering and Design*, **279**, pp. 182–188 (2014).

13. C. E. Estrada-Pérez, Y. A. Hassan, B. Alkhudhiri, and J. Yoo, "Time-resolved measurements of liquidvapor thermal interactions throughout the full life-cycle of sliding bubbles at subcooled flow boiling conditions," *International Journal of Multiphase Flow*, **99**, pp. 94–110 (2018).

14. L. Z. Zeng, J. F. Klausner, D. M. Bernhard, and R. Mei, "A unified model for the prediction of bubble detachment diameters in boiling systems-II. Flow boiling," *International Journal of Heat and Mass Transfer*, **36** (9), pp. 2271–2279 (1993).

15. T. Mazzocco, W. Ambrosini, R. Kommajosyula, and E. Baglietto, "A reassessed model for mechanistic prediction of bubble departure and lift off diameters," *International Journal of Heat and Mass Transfer*, **117**, pp. 119–124 (2018).

16. A. Richenderfer et al., "Investigation of subcooled flow boiling and CHF using high-resolution diagnostics," *Experimental Thermal and Fluid Science*, **99**, pp. 35–58 (2018).

17. A. Kossolapov, *Experimental Investigation of Subcooled Flow Boiling and CHF at Prototypical Pressures of Light Water Reactors*, PhD thesis, Massachusetts Institue of Technology, 2021.

18. J. Magnaudet and D. Legendre, "The viscous drag force on a spherical bubble with a time-dependent radius," *Physics of Fluids*, **10** (3), pp. 550–554 (1998).

19. D. Legendre, C. Colin, and T. Coquard, "Lift, drag and added mass of a hemispherical bubble sliding and growing on a wall in a viscous linear shear flow," *Philosophical Transactions of the Royal Society A: Mathematical, Physical and Engineering Sciences*, **366** (1873), pp. 2233–2248 (2008).

20. P. Shi, R. Rzehak, D. Lucas, and J. Magnaudet, "Hydrodynamic forces on a clean spherical bubble translating in a wall-bounded linear shear flow," *Physical Review Fluids*, **5** (2020).

21. R. Mei and J. F. Klausner, "Unsteady force on a spherical bubble at finite Reynolds number with small fluctuations in the free-stream velocity," *Physics of Fluids*, **4** (1), pp. 63–70 (1993).

22. V. Scheiff, F. Bergame, J. Sebilleau, P. Ruyer, and C. Colin, "Experimental study of steady and transient subcooled flow boiling," *International Journal of Heat and Mass Transfer*, **164** (2021).

23. C. W. M. van der Geld, "The dynamics of a boiling bubble before and after detachment," *Heat and Mass Transfer*, **45**, pp. 831–846 (2009).

24. H. Lamb, *Hydrodynamics*, Cambridge University Press (1895).

25. M. S. Plesset and S. A. Zwick, "The Growth of Vapor Bubbles in Superheated Liquids," *Journal of Applied Physics*, **25** (4), pp. 493–500 (1954).

26. P. Guan, L. Jia, L. Yin, and Z. Tan, "Bubble departure size in flow boiling," *Heat and Mass Transfer* (2014).

27. W. Frost and G. S. Dzakowic, "An extension of the method of predicting incipient boiling on commercialy finished surfaces," *ASME paper* (1967).

28. H. Reichardt, "Vollstndige Darstellung der turbulenten Geschwindigkeitsverteilung in glatten Leitungen," *Zeitschrift fr Angwandte Mathematik und Mechanik*, **31** (7), pp. 208–2019 (1951).

29. M. Bucci, J. Buongiorno, and M. Bucci, "The not-so-subtle flaws of the force balance approach to predict the departure of bubbles in boiling heat transfer," *Physics of Fluids*, **017110** (33) (2021).